SF 298 MASTER COPY KEEP THIS COPY FOR REPRODUCTION PURPOSES

REPORT DOCUMENTATION PAGE

Form Approved
OMB NO. 0704-0188

1. AGENCY USE ONLY *(Leave blank)*	2. REPORT DATE	3. REPORT TYPE AND DATES COVERED
	6-7-96	Final 3/1/93 - 2/29/96

4. TITLE AND SUBTITLE
New Mechanisms and New Materials for Organic Optical Nonlinearity

5. FUNDING NUMBERS
F49620-93-1-0199
2303/CS
61102F

6. AUTHOR(S)
N. Peyghambarian, S. Mazumdar, and N. Armstrong

7. PERFORMING ORGANIZATION NAMES(S) AND ADDRESS(ES)
Optical Sciences Center
University of Arizona
Tucson, AZ 85721-0094

8. PERFORMING ORGANIZATION REPORT NUMBER
AFOSR-TR-96
0331

9. SPONSORING / MONITORING AGENCY NAME(S) AND ADDRESS(ES)
AFOSR/NL
110 Duncan Ave, Suite B115
Bolling AFB DC 20332-8080

10. SPONSORING / MONITORING AGENCY REPORT NUMBER

11. SUPPLEMENTARY NOTES
The views, opinions and/or findings contained in this report are those of the author(s) and should not be construed as an official Department of the Army position, policy or decision, unless so designated by other documentation

12a. DISTRIBUTION / AVAILABILITY STATEMENT
Approved for public release; distribution unlimited.

12 b. DISTRIBUTION CODE

13. ABSTRACT *(Maximum 200 words)*

This program has been extremely successful with over 50 publications and presentations (see the enclosed publication list). During this period, we had two publications in Nature, two in Physical Review Letters, and the remaining publications in other reputed journals. Both Nature and the American Chemical Society decided to have a news release on our photorefractive results. Not only did we obtain the most efficient photorefractive polymer to date, but we also demonstrated and reported the first observation of excitonic strings in an organic crystal. The following is a summary of our achievements.

14. SUBJECT TERMS
organic, nonlinear, polymer

15. NUMBER IF PAGES
28

16. PRICE CODE

17. SECURITY CLASSIFICATION OR REPORT	18. SECURITY CLASSIFICATION OF THIS PAGE	19. SECURITY CLASSIFICATION OF ABSTRACT	20. LIMITATION OF ABSTRACT
UNCLASSIFIED	UNCLASSIFIED	UNCLASSIFIED	UL

Final Report on Contract #F49620-93-1-0199

Program Director: Dr. Charles Lee

New Mechanisms and New Materials for Organic Optical Nonlinearity

N. Peyghambarian, S. Mazumdar, and N. Armstrong

University of Arizona

Tucson, AZ 85721

Achievements in the Last Three Years

This program has been extremely successful with over 50 publications and presentations (see the enclosed publication list). During this period, we had two publications in Nature, two in Physical Review Letters, and the remaining publications in other reputed journals. Both Nature and the American Chemical Society decided to have a news release on our photorefractive results. Not only did we obtain the most efficient photorefractive polymer to date, but we also demonstrated and reported the first observation of excitonic strings in an organic crystal. The following is a summary of our achievements.

A. Photorefractive Polymers

1. Material development

- First demonstration of photorefractivity in a side-chain polymer containing carbazole and the second-order tricyanovinylcarbazole moieties as pendant groups (1993).
- Development of a polymer composite that simultaneously showed photorefractivity and other gratings due to the photo-isomerization properties of the nonlinear dye. Comparison of two types of recording mechanisms in a PVK based material doped with the dye Disperse Red 1 (1994).
- Development of highly efficient guest/host polymers based on PVK and doped with several nonlinear azo dyes. Demonstration of nearly 100% diffraction efficiency and corresponding refractive index changes close to 1%. Demonstration of net gain coefficients in excess of 200 cm^{-1} (to be compared with 50 cm^{-1} for the best inorganic photorefractive crystals) (1995).

2. Evidence of new mechanisms in photorefractive polymers

- Clear identification of the orientational enhancement mechanism in low T_g photorefractive polymers. Measurement of the relative contributions of the electro-optic effect and the modulated birefringence

due to the reorientation of the chromophores by the internal space-charge field. Demonstration of the strong birefringence mechanism for composites doped with the dye DMNPAA.

- Development of a frequency-dependent ellipsometry measurement technique that clearly identifies the first, second, and third-order contribution to the total signal in low T_g photorefractive polymers.
- Observation of non-Bragg orders and demonstration of the phase-conjugated properties of the new generated diffraction orders.

3. Demonstration of several photonic applications with photorefractive polymers

- Holographic storage with low-power semiconductor laser diodes.
- Demonstration of an optical correlator with photorefractive polymers.
- Demonstration of time-average interferometry.

B. Third-Order Optical Nonlinearity

1. Mechanism of third-order nonlinearity

- Joint experimental-theoretical study of the electroabsorption of a DCH-polydiacetylene. Identification of the essential states that determine the bulk of the optical nonlinearity of these systems (1993).
- Demonstration of multiexciton strings in an organic charge-transfer solid by pump-probe spectroscopy. Development of theory of multiexcitons (1994).

2. Nonlinear optical materials

- Theoretical and experimental demonstration of excitons in poly(para-phenylenevinylene). Determination of the exciton binding energy.
- Development of improved growth techniques using organic-inorganic MBE to produce highly ordered fluoroaluminum and chloroindium phthalocyanine (FAlPc and ClInPc) thin films for nonlinear optical studies.
- Femtosecond pump-probe studies of FAlPc and ClInPc thin films. Theoretical determination of the mechanism of photo-induced absorption in these systems.
- Determination of the frequency-dependent third harmonic generation spectrum of epitaxial chloro-indium phthalocyanine. Theory of third harmonic generation in phthalocyanines.
- Determination of the frequency-dependent third harmonic generation spectrum of the PtCl MX chain.

Photorefractive Polymers[1-9]

Since demonstrating near 100% diffraction efficiency and high net optical gain (>200 cm^{-1}) in our material,[1-6] we have continued to characterize its properties and have demonstrated some practical applications. Our work involves the guest/host photorefractive polymer composite DMNPAA:PVK:ECZ:TNF 50:33:16:1 %wt, which is a mixture of the photoconducting polymer poly(N-vinylcarbazole) (PVK) doped with the strong acceptor 2,4,7-trinitro-9-fluorenone (TNF), which forms a charge-transfer complex with PVK, mixed together with the electro-optic chromophore 2,5-dimethyl-4-(p-nitrophenylazo)anisole (DMNPAA), and with N-ethylcarbazole (ECZ) added as a plasticizer. Measurements of the refractive index modulation, the optical gain as a function of applied electric field, and light intensity, as well as measurements of the dynamics of the grating build-up and decay, further our efforts to understand the properties of our material. Also, frequency-dependent measurements of the electro-optic response support our model calculations, which indicate that periodic poling of the chromophores by the internal space-charge field provides a major contribution to the total refractive index modulation (the so-called orientational enhancement effect). Applications we have demonstrated so far include a matched-filter optical correlator, holographic data storage, and dynamic holographic interferometry.

A. Characterization

1. Refractive Index Modulation and Optical Gain as a Function of Applied Electric Field

The amplitude of the refractive index modulation (Δn) was deduced from measurements of the diffraction efficiency (η) (four-wave-mixing experiments using Kogelnik's coupled-wave model for diffraction in thick holograms. The diffraction efficiency was defined to be the ratio of the power of the diffracted beam to that of the probe beam before entering the sample. Amplitudes of $\Delta n = 0.007$ were observed for an applied field of 90 V/μm. Complete diffraction of the probe beam occurred at $\Delta n = 0.0026$ (the maximum diffraction efficiency of 86% is limited by reflection and absorption losses). As the index modulation increases further, the diffraction efficiency shows a periodic behavior, as predicted by theory. The optical gain measurements were taken from two-beam-coupling experiments. Two-beam coupling leads to asymmetric energy transfer between two coherent beams, and it requires the presence of a phase shift between the light intensity grating and the induced index grating, which is the signature of the photorefractive effect. Optical gain of more than 200 cm^{-1} was observed for p-polarized beams at an

applied field of 90 V/μm, while that for s-polarized beams was -40 cm^{-1} at 90 V/μm. Note the negative sign of the optical gain for s-polarized beams. This indicates that field-induced birefringence is the dominant contribution to the refractive index modulation in our material.

2. Refractive Index Modulation as a Function of Light Intensity

In order to determine the saturation intensity of the holographic recording in our material, we varied the intensity of the writing beams in our four-wave-mixing setup for a given applied electric field (80 V/μm) and observed saturation of the index modulation at around 3 W/cm^2, which agrees with our photorefractive model for polymers.

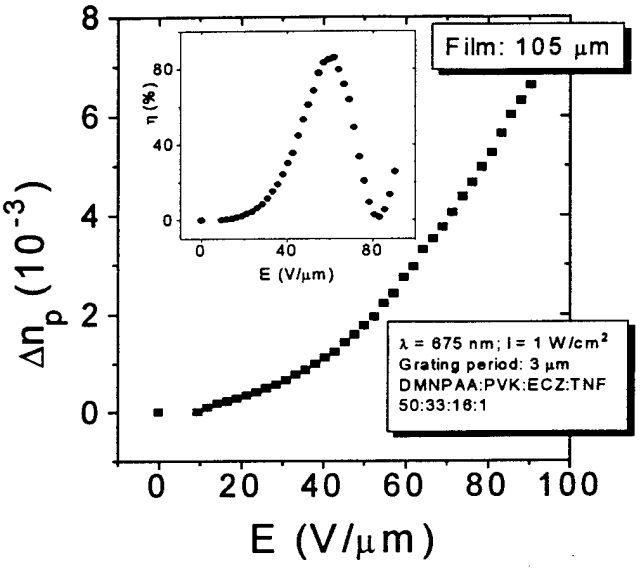

Figure 1. Refractive index modulation Δn versus applied electric field. Inset: Diffraction efficiency η versus applied electric field.

3. Dynamics of Grating Build-up and Decay

The dynamics of grating formation and erasure in photorefractive polymers is complex and involves several time constants that arise from different physical processes. In order to better understand the temporal behavior of our material, we observed the build-up of the diffraction efficiency in our four-wave-mixing setup after the second of the two writing beams was turned on, while the applied electric field and the first writing beam were already on. A multiple exponential fit shows several time constants in the grating build-up time, ranging from 50 ms to minutes. The rise time with the largest weighting factor is

around 0.5 s, which does not depend strongly on the light intensity over the range from 10 mW/cm^2 to 1 W/cm^2.

4. Frequency Dependence of the Electro-optic Response

We measured the electro-optic response of our material using the crossed polarizer technique, where the sample is placed between two crossed polarizers, and a Babinet-Soleil compensator is used to adjust the relative phase between s and p components of the polarization. Linear polarized light from the first polarizer makes a 45° angle with respect to the plane of incidence of the sample, such that the beam passing through the sample has equal s- and p-polarization components. An applied field across the sample induces a change in the index of refraction of the material due to its electro-optic property. The index change is different for s- and p-polarizations, hence the light leaving the sample is changed from linear to elliptical polarization. The amount of change in the polarization is observed as a change in the intensity of the light that passes through the second polarizer. Using the model of Teng and Man,[7] we calculate the effective electro-optic coefficient from our measurements of the light intensity modulation that results from a modulation of the applied electric field across our material. We observe two regimes in the frequency dependence of the electro-optic response. At high frequencies (above 100 Hz) we observe that the EO response has decreased and leveled off to a value around 0.2 pm/V^2, while at low frequencies (below 0.1 Hz) we observe the EO response has increased and leveled off to a value around 4.3 pm/V^2. In the high frequency regime the molecules are unable to reorient themselves quickly enough to follow the changing applied field, and hence, the EO response that we observe is due solely to the intrinsic EO property of the material. At the low frequency regime the molecules can reorient themselves to follow the changing applied field; the changing oriented alignment of the molecules produces a birefringence contribution to the observed EO response and also doubles the EO properties. It is clear that at low frequencies the major contribution to the EO response in our material is due to the induced birefringence.

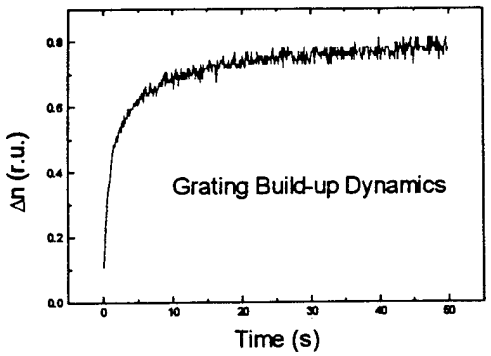

Figure 2. Grating writing dynamics; refractive index modulation Δn versus time.

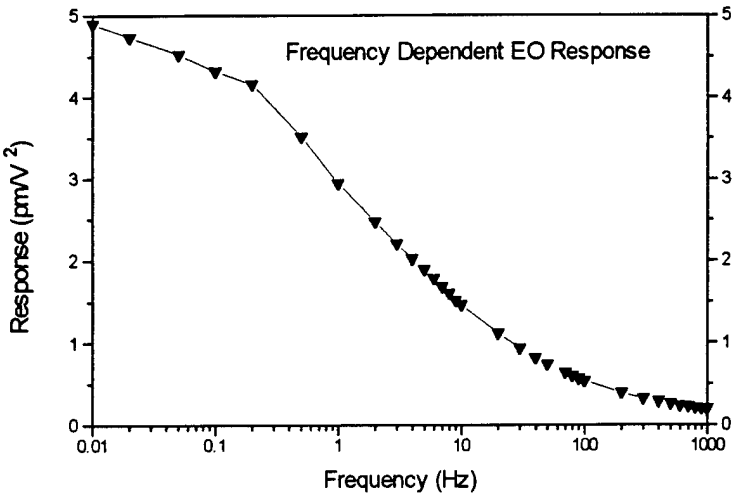

Figure 3. Electro-optic response versus frequency of the modulated electric field.

B. Applications

1. Matched-Filter Four-Wave-Mixing Optical Correlator[8]

We used our polymer as the nonlinear optical material in a matched-filter image correlator in collaboration with the University of California, Santa Barbara, Institute for Polymers and Organic Solids. The device involves two time regimes; the time required to reprogram the reference image (by erasing the old image and writing a new one) and the time required to diffract a test image from the grating and detect its signal. Reprogramming the reference image is limited by the grating decay and build-up time in our material, which was sub-second in this demonstration. Once the reference grating is written, the diffraction of the test image is essentially instantaneous, so the time to recognize a test image is not limited by our material. This experiment demonstrated that our material could be used efficiently in optical image processing applications.

2. Holographic Data Storage[4]

We demonstrated storing two-dimensional and three-dimensional optical images in our material by (a) placing a photographic slide in one of the writing beams, and (b) replacing one of the writing beam mirrors with a three-dimensional reflecting surface (i.e., a new penny), respectively. A picture of the reconstructed three-dimensional hologram of a penny using our material appeared on the cover of the January 1995 issue of Physics Today.

3. Dynamic Holographic Interferometry[9]

We also demonstrated dynamic holographic interferometry by replacing one of the writing beam mirrors with a flexible reflecting film that was excited acoustically by a loudspeaker. The vibrational modes of the flexible mirror were recorded holographically in our material and could be read out in real time.

Organic Nonlinear Optical Materials

A. Instrumentation

In 1994 we constructed a combination of optical parametric generator/amplifiers (OPG/OPA) based on beta barium borate (BBO) crystals. It afforded us a widely tunable intense laser source to conduct nonlinear laser spectroscopy on organic compounds. The device was pumped by the third harmonic output (355 nm) from a picosecond Nd:YAG laser with a pulse width of 35 ps, 10 mJ/pulse, and 10 Hz repetition rate. The wavelength tuning range of our OPG/OPA was from 450 nm to 2.3 micron, effectively covering the entire visible and near infrared regions. Following the construction of the OPG/OPA, we built a third harmonic generation setup which is capable of measuring third-order optical nonlinear susceptibility $\chi^{(3)}(-3\omega;\omega,\omega,\omega)$ in a wide wavelength range. The experimental arrangement is shown in Fig. 4, where THG is the third harmonic generator installed in the Nd:YAG laser, and PD stands for photodiode detector. The sample is mounted on a rotational stage so that Maker fringes can be measured during the third harmonic generation experiment. The signal (infrared) beam is focused on the sample by a microscope objective. This tight focusing scheme ensures that the contribution from the air to the third harmonic signal is negligible. The third harmonic signal generated by the sample is collected by the monochromator and detected by a photomultiplier tube. The idler (visible) beam from the OPG/OPA is sent to a photodiode detector for monitoring the laser pulse fluctuation. The data is stored in a two-channel boxcar averager for data processing. The experimental wavelength range of our wavelength tunable third harmonic generation setup is from 850 nm to 1.8 micron (limited by the sensitivity of our photodetector in the IR region).

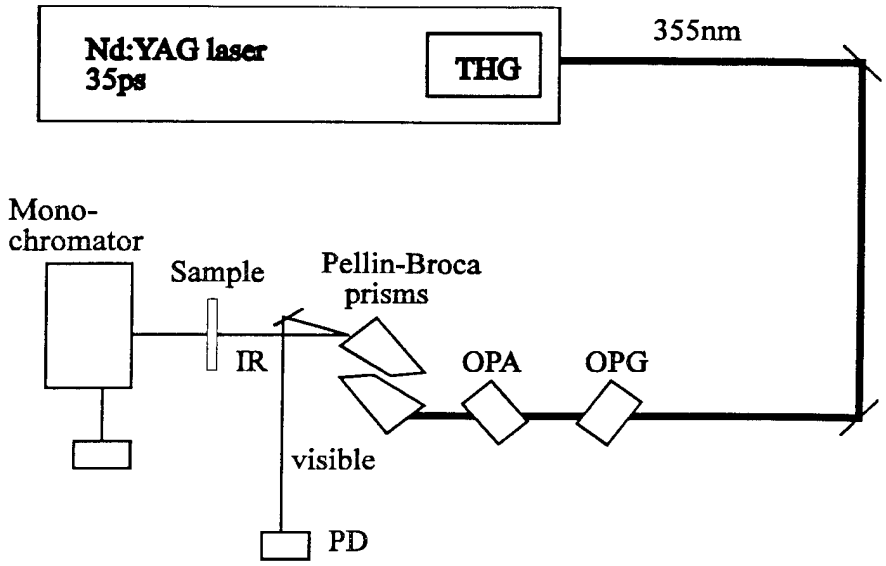

Figure 4. Diagram of frequency tunable third harmonic measurement.

B. Spectra of $\chi^{(3)}(-3\omega;\omega,\omega,\omega)$ of Epitaxially Grown Metal Phthalocyanine Films

During this most recent research period we have continued to actively explore the growth and characterization of multilayer phthalocyanine thin films[10-13] and to correlate their linear optical properties with their nonlinear optical properties.[14] Of particular note has been the mastery of the growth conditions in OMBE to produce highly ordered fluoroaluminum phthalocyanine (FAlPc) thin films which add to the family of epi-layers that have become candidates for characterization by femtosecond differential absorbance spectroscopy and direct measurements of the wavelength dependence of $\chi^{(3)}$.[10,13] Figure 5 summarizes our current understanding of the way in which subtle changes in packing architecture in the epi-Pc film can control their Q-band absorbance response.

Spectra (a) and (b) represent two different packing configurations for a trivalent metal Pc, such as ClInPc, showing how a small change in ring-ring displacement in the second and third layers of these highly ordered materials causes a significant increase in the red-shifting response of the Q-band. The absorptivity of the "Phase II" material is higher than for the "Phase III" material and, it is anticipated, will show a correspondingly higher $\chi^{(3)}$. The $\chi^{(3)}$ for the Phase III system was measured during this last funding period and shows that the nonlinearity tracks the absorbance but shows additional two- and three-photon

resonance features.[14] Work is in progress to measure these same types of responses with Phase II thin films.

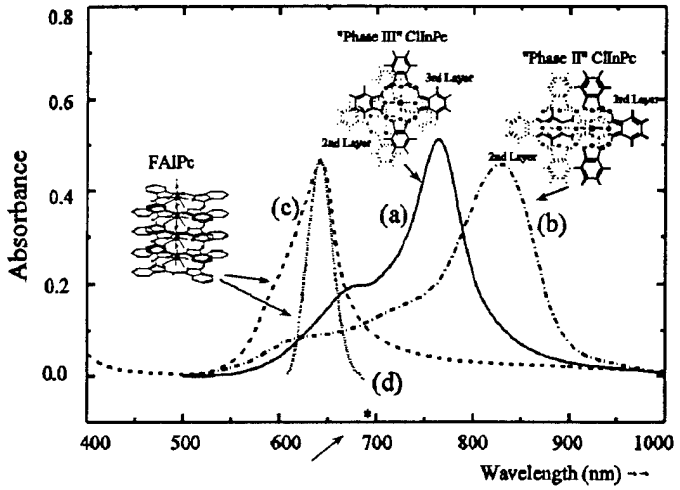

Figure 5. Absorbance spectra of various phthalocyanine thin films. (a) ca. 50 monolayers of ClInPc epitaxially grown on $SnS_2(0001)$; (b) several monolayers of ClInPc grown on single crystal sapphire; (c) ca. 50 monolayers of FAlPc on $SnS_2(0001)$ at substrate temperature below 100°C; (d) ca. 50 monolayers of FAlPc on $SnS_2(0001)$ at substrate temperatures above 150°C, RHEED analysis verifies real epitaxy with the growth of this film.

Spectra (c) and (d) show the FAlPc spectra for two types of film grown on the basal (0001) planes of freshly cleaved SnS_2. Spectrum (d) is obtained when the single crystal is held at a sufficient temperature during film growth (150°C) to create true single crystal domains (with flat-lying Pc rings) over a micron distance scale. The Q-band spectrum, in addition to being strongly blue-shifted due to the cofacial linear stacking pattern, also has a FWHM of ca. 50-60 nm, which is unprecedented for a molecular crystal. Work is now in progress to create this type of ordering on optical quality substrates such as Kbr(001), and to extend the study of nonlinear optical effects to this type of Pc stacking pattern. Work is now also in progress to produce a series of Pc/spacer (e.g., perylene, pentacene derivatives, etc.,[11,12] multilayers on similar substrates to further investigate the energy/charge transfer processes which can occur on the

picosecond time scale following excitation in either the Pc or spacer layer. The Pc's films mastered during this funding period are excellent candidates for such studies.

Phthalocyanine compounds have attracted considerable interest due to their unique structure and their structure/property relation related to the center metal substitution.[15,16] In Neal Armstrong's laboratory, epitaxially grown chloro-indium-phthalocyanine (Cl-In-Pc) thin films with various crystalline phases have been successfully fabricated.[17] Specifically, Cl-In-Pc films with epitaxial phases II and III are available for nonlinear optics experiment in our project. Using our wavelength tunable third harmonic generation setup, we have obtained the spectra of $\chi^{(3)}(-3\omega;\omega,\omega,\omega)$ of Cl-In-Pc in both epitaxial phase II and phase III in the wavelength range of 900-nm - 1.8 micron (fundamental wavelength). The objective of this experiment was to obtain a detailed spectrum of third-order optical nonlinear susceptibility in the wavelength region of interest and to discern the effect of crystalline structure of Cl-In-Pc on its nonlinear optical properties. In this fiscal year we have succeeded in obtaining spectra of Cl-In-Pc films. We have observed two-photon absorption peaks in the transparent region of Cl-In-Pc, and, furthermore, the positions of the two-photon peaks are found to be dependent on the crystalline structure of the phthalocyanine.[18]

The molecular arrangements of crystalline phases of Cl-In-Pc are shown in Fig. 6. We found experimentally that freshly cleaved KBr crystal surface is conducive to the growth of epitaxial phase III, while a clean sapphire surface is favorable for that of epitaxial phase II. A picosecond third harmonic generation experiment was done on both of these samples. The experiment was conducted in air and no sample damage was observed. Third harmonic signals were extracted from the Maker fringes measurement, and corrections due to linear absorption were taken into account in the calculation of $\chi^{(3)}(-3\omega;\omega,\omega,\omega)$ values. Experimental curves of the dispersions of third-order nonlinear optical susceptibility of Cl-In-Pc films in epitaxial phases II and III are depicted in Fig. 7.

In Fig. 7 the square dots are experimental data of $\chi^{(3)}(-3\omega;\omega,\omega,\omega)$, and the solid lines are linear absorption curves of epitaxial phases II and III in the respective wavelength regions. Note that the $\chi^{(3)}$ data are plotted against third harmonic wavelengths. The peak in third harmonic signal in the long wavelength region is the 3-photon resonance to the B band (the absorption peak in the 300-nm - 400-nm region) of Cl-In-Pc, as depicted in the figures. In addition, there occur two other resonances. These two are most clear in the epitaxial phase III, where they occur at third harmonic wavelengths 415 nm and 500 nm [see Fig. 7(b)]. Our theoretical analysis (see below) indicates that at least one of these additional resonances is a two-photon resonance. It is intriguing to note that there is a shift of the two-photon resonance peaks in different epitaxial phases (II and III), as shown in Fig. 7. It is instructive to recall that the exciton shift (Davidov splitting) observed in the linear absorption spectra of phthalocyanines has the same general trend

as in the two-photon resonance shift in our experiment, with respect to different epitaxial phases (see Ref. 17). Thus, we observed the exciton effect on 2-photon accessible levels.

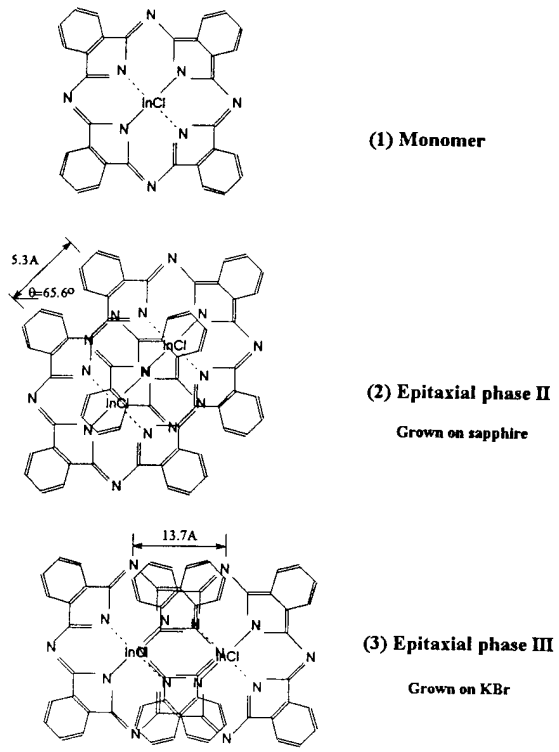

Figure 6. Crystalline structures of In-Cl-phthalocyanine.

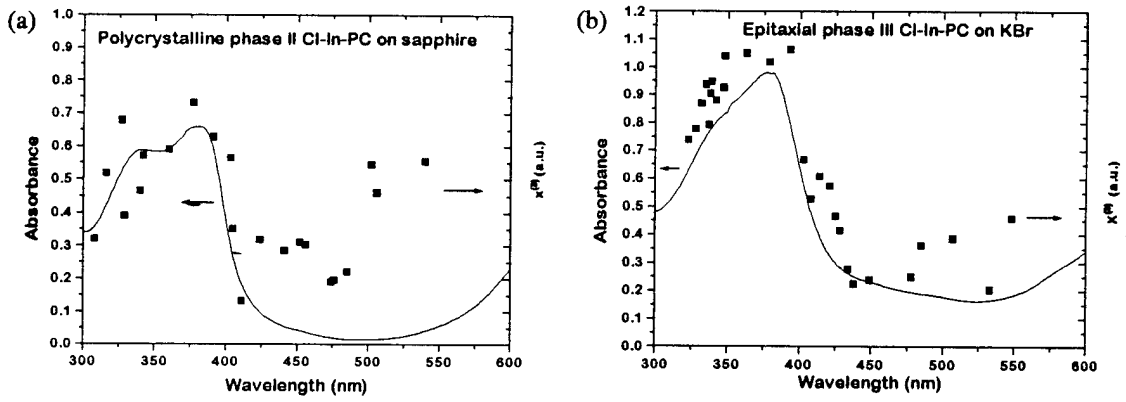

Figure 7. $\chi^{(3)}$ $(-3\omega;\omega,\omega,\omega)$ spectra of Cl-In-Pc. (a) Epitaxial phase II. (b) Epitaxial phase III.

Theoretical modeling of the THG of M-Pc was done within the Pariser-Parr-Pople model using the singles-CI approximation. Since the central atom in our case is not a transition metal and, therefore, has a closed shell, the calculation was done for the Pc ligand only. Within the singles-CI approximation the Q-band and B-band absorptions occur at 1.41 eV and 3.58 eV, respectively. In addition, we find a weak B' absorption at 2.35 eV. Calculations of the molecular hyperpolarizability tensor were done using the standard sum-over-states approach, and from the tensor components the average hyperpolarizability γ_g was calculated. A plot of the average molecular hyperpolarizability is shown in Fig. 8. Note that a two-photon resonance is observed below the three-photon resonance to the B-band, in agreement with the experimental observation. Whether or not the three-photon resonance to the B' band (M/3 in Fig. 8) would be observable in experiment, and whether additional two-photon resonances below the three-photon resonance would occur within the theory if higher order CI is taken into account, are currently being investigated.

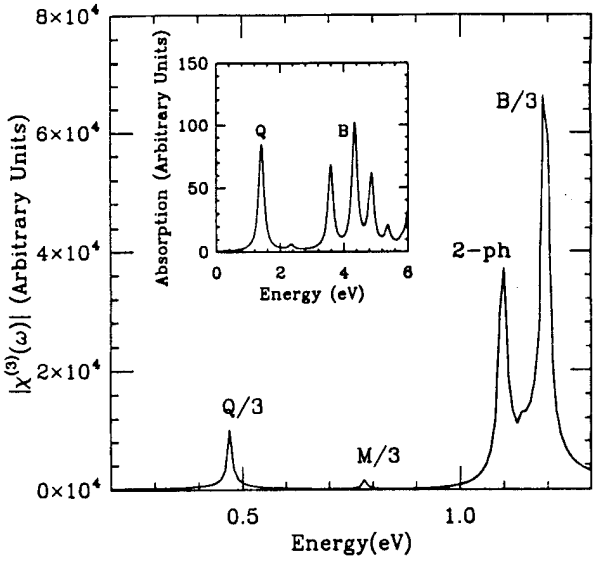

Figure 8. Calculated γ_g (-3ω;ω,ω,ω) for the Pc^{2-} molecule within the PPP model. In addition to the three-photon resonance at energy B/3 (where B is the threshold energy of the B-band), a strong two-photon resonance (2-ph) and a very weak three-photon resonance M/3 are found. The three-photon resonance Q/3 due to the Q-band is outside the experimental frequency range. The calculated PPP-SCI absorption is shown as an inset.

C. Spectrum of $\chi^{(3)}$(-3ω;ω,ω,ω) of Quasi-1-dimensional Pt Complex

Utilizing our versatile wavelength tunable third harmonic generation setup, we have measured the spectrum of $\chi^{(3)}$(-3ω;ω,ω,ω) of quasi-1-dimensional halogen-bridged mixed-valence Pt complex. The work was done in collaboration with Drs. Basil Swanson and Duncan McBranch of Los Alamos National Laboratory. The chemical formula of the sample in our experiment is

$[Pt(ethylenediamine)_2][Pt(ethylenediamine)_2Cl_2](ClO_4)_4$. The objective of this experiment was to investigate charge transfer effect on the third-order optical nonlinearity and to explore the possibility of using third harmonic generation as a spectroscopic tool.[21] Preliminary results in the wavelength range 330 nm - 550 nm have shown several distinct spectroscopic features near the charge transfer peak of the complex. Currently, we are undertaking the task of improving our experimental measurement and finding a theoretical explanation of the observed features.

D. Excitons in Polyphenylenes[22,23]

The bulk of the theoretical work on third-order optical nonlinearities in B-conjugated polymers has involved the simplest linear chain systems, i.e., the polyacetylenes and the polydiacetylenes. Most conjugated polymers, however, are structurally different and contain aromatic rings. One of our goals is to investigate the effect of such structural variations on optical nonlinearity. To this end we have begun an investigation of the polyphenylenes, a typical member of which is poly(para-phenylenevinylene) (PPV). As an initial step toward probing the mechanism of optical nonlinearity in this system, we have focused on the electronic structure of this system and its linear optical absorption in the past year. We have found strong evidence that optical absorption in this system is due to an exciton which is strongly confined and has a large binding energy.

In Fig. 9(a) we give the band structure of PPV, with the unit cell as an insert. Here the d and d* bands are completely delocalized, but the two flat bands ℓ and ℓ^* are localized with nonzero electron densities only on the carbon atoms 2, 3, 4, and 5 (see inset). An explicit calculation[22,23] indicates that the bands below R and above R^* participate weakly in absorption. Within band theory, one then expects three absorptions, corresponding to the transitions (i) $d_1 \rightarrow d^*_1$ (ii) $d_1 \rightarrow \ell^*$ and $\ell \rightarrow d_1^*$ (note: these are degenerate), and (iii) $\ell \rightarrow \ell^*$. Note that the transitions (ii) should occur at an energy that is exactly at the center of the two other transition energies (i) and (iii). The calculated absorption spectrum within band theory is shown in Fig. 9(b).

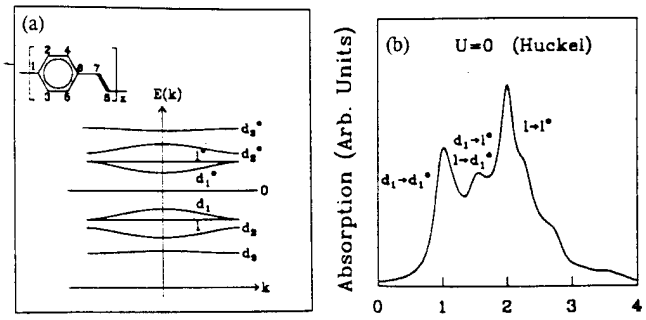

Figure 9. (a) Band structure of PPV with the unit cell shown as an inset. (b) Calculated absorption within band theory.

Figure 10(a) shows the experimental absorption spectrum of poly[2-methoxy,5-(2'-ethyl-hexyloxy)-1,4 phenylenevinylene] (MEH-PPV). The absorption is clearly different from that predicted within band theory [Fig. 9(b)]. Neither of the two weaker peaks occur at the center of the two strong peaks at 2.4 and 5.8 eV. We have found that the only way to fit the experimental spectrum is to assume moderately strong Coulomb interactions within a Pariser-Parr-Pople type Hamiltonian for PPV. Our best fit within the correlated model to the optical absorption of an 8-unit capped oligomer is shown in Fig. 10(b). Within the correlated model, the lowest optical state is an exciton with a binding energy as large as 0.9 ± 0.15 eV. The arrows on the x-axis indicate the threshold of the continuum band, determined by two independent methods.[22,23] The strong exciton binding comes both from the moderate Coulomb interactions, as well as the effectively large bond dimerization in the structure of PPV.

We have made preliminary calculations of optical nonlinearity which indicate that in spite of the complex structure, the mechanism of nonlinearity in this system is similar to that in the linear chain polydiacetylenes.[24-2713] In particular, the optical exciton has a very large dipole coupling with an even-parity exciton that occurs above the optical exciton but below the continuum.[24-27] The even-parity exciton, forbidden in linear absorption, plays a strong role in nonlinear optics. For example, it acquires oscillator strength from the exciton in electro-absorption and becomes visible,[28] as shown in Fig. 11.

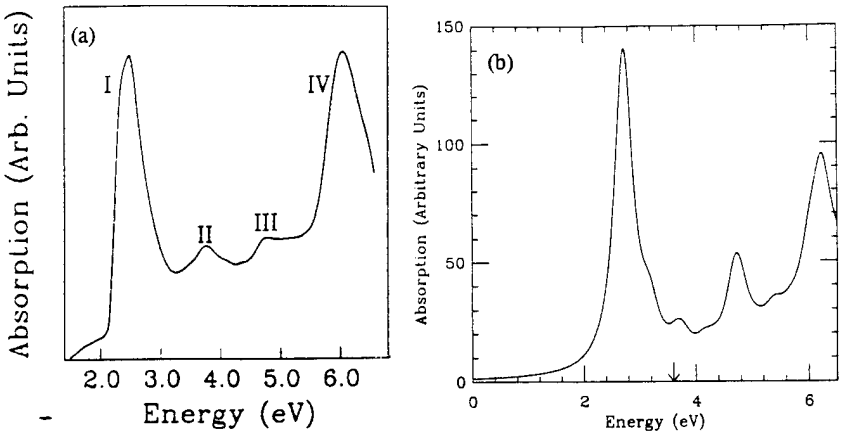

Figure 10. (a) Experimental absorption spectrum of a thin film of MEH-PPV. (b) Calculated absorption spectrum within the Coulomb correlated model. Now the lowest optical state is an exciton. The arrows on the x-axis give the location of the continuum threshold determined by two independent approaches.

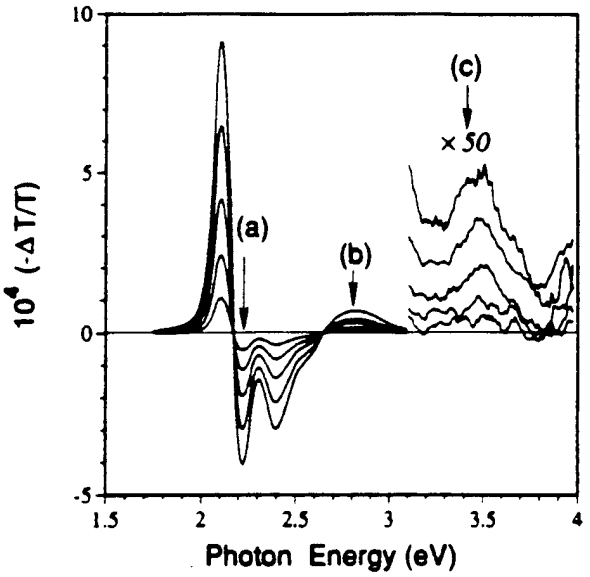

Figure 11. Electroabsorption of MEH-PPV. In addition to the Stark shift of the exciton [feature (a)], there is a field-induced feature (b) that has been assigned to a forbidden even-parity exciton.

E. New Nonlinear Optical Channel: Biexcitons[29,30]

Theoretical work on third-order optical nonlinearity in B-conjugated systems has been limited to nonlinear optical channels involving the optical exciton, a dominant even-parity exciton, and the threshold of the conduction band.[24-27] We have recently shown that stable biexcitons exist within the Coulomb-correlated models for π-conjugated polymers with standard Coulomb parameters, and therefore, a new nonlinear optical channel involving the exciton and the biexciton becomes possible.[24,25] Such a channel can explain a picosecond (ps) photo-induced absorption (PA) that has been seen in a number of polymers over the years[31-34] and that had remained a mystery until recently.

Our theoretical work is within the extended Hubbard model:

$$H = U \sum_i n_{i,\uparrow} n_{i,\downarrow} + V \sum_i (n_i - 1)(n_{i+1} - 1) - t \sum_{i,\sigma} [1 - (-1)^i \delta][c^+_{i,\sigma} c_{i+1,\sigma} + c^+_{i+1,\sigma} c_{i,\sigma}] \quad (1)$$

Here $C^+_{i\sigma}$ creates an electron of spin σ at site i. Only the last term occurs in the Huckel model, to which we have added the on-site and nearest neighbor electron correlations, U and V. The direct demonstration of stable biexcitons within Eq.(1) would require the determination of the two-exciton continuum above the biexciton and proof of the formation of bound states below the continuum. Since, however, such calculations have to include configuration interaction with at least quadruple excitations, and are therefore

limited to short chains (10 atoms), and since a true continuum can occur only in long chains, the direct demonstration of the biexciton is not possible and an indirect approach is called for.

We have developed such an indirect approach using a physical, intuitive picture. We imagine a long chain with the first exciton already formed. For stable biexcitons to exist, the second exciton can occur in only one of two "spots," to the left or to the right of the first exciton, at a distance such that binding can occur. This is shown schematically in Fig. 12(a). In contrast, the second exciton in a two-exciton continuum can appear at arbitrary relative distance from the first exciton. Thus, in a long chain, the two-exciton continuum states are superpositions of a very large number of basis functions, while the biexciton is constructed out of a few. The density of states is consequently much larger at the continuum edge, and we expect that the strength of the absorption from the $1B_u$ exciton to the two-exciton continuum edge is larger than the oscillator strength of the absorption to the biexciton. A schematic of the absorption strengths from the one-exciton to the two-exciton states is shown in Fig. 12(b). Note that this is opposite the absorption from the ground state to the exciton and the one-electron-one-hole (1e-1h) continuum, where the absorption to the exciton is strong, and to the continuum is weak. Based on the above picture, we can argue that the observation of a weaker transition strength from the $1B_u$ exciton to the lowest two-exciton state than that to a higher energy two-exciton state is a signature of exciton binding.

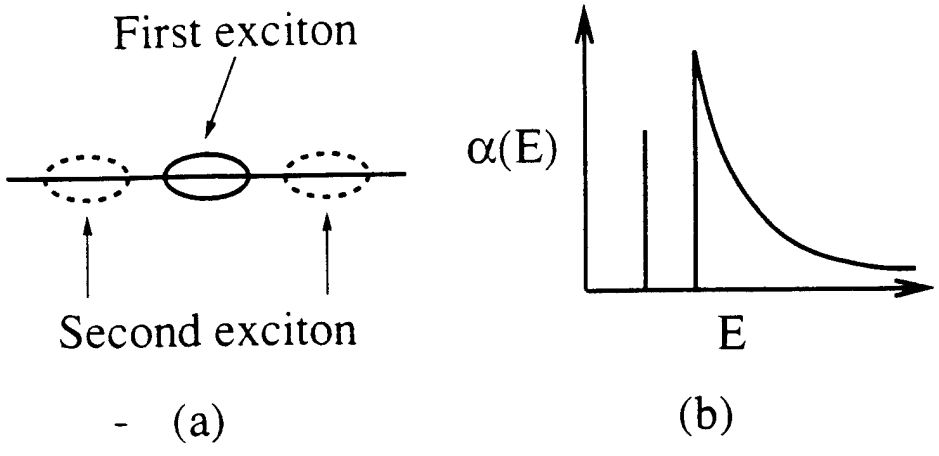

Figure 12. (a) Location of the second exciton (one of two dashed ellipses), relative to the first (solid ellipse) in a biexciton. In a two-exciton continuum state the second exciton occurs at arbitrary distance from the first exciton. (b) Schematic of the absorption from the $1B_u$ to the two-exciton states in the case of biexciton formation.

We establish the validity of this criterion by examining the strong coupling limit of very tightly bound excitons. Consider the case of U >> V >> t. The ground state of the half-filled band has all sites singly

occupied. The exciton states are even- and odd-parity linear combinations of configurations ....11120111..., where the numbers denote site occupancies. The 1e-1h continuum consists of all states in which the double occupancy (particle) and the empty site (hole) are separated by more than one site (for example, ..11211..1011..). The biexciton states consist of configurations ...1112020111..., which occur at energy 2U-3V, while the lowest two-exciton continuum states have occupancies ...12011..12011..., and occur at energy 2U-2V. Thus, in the strong coupling limit, the biexciton binding energy and the exciton binding energy are the same, i.e., V. Figure 13(a) shows the exact energy states for a periodic ring of N = 10 sites for U/t = 50, V/t = 15, and δ = 0.1. Finite size effects are minimal for these very large Coulomb parameters, and exciton states at U-V, the 1e-1h continuum centered at U, the biexciton at 2U-3V and the two-exciton continuum at 2U-2V are all distinct. Only one of the exciton states at U-V has large dipole coupling with the ground state. In Fig. 13(b) we show the normalized dipole couplings between the optical exciton and all two-exciton states. Note that the dipole coupling with the biexciton B at 2U-3V is smaller than the dipole coupling with the state C at the edge of the two-exciton continuum, in agreement with our physical criterion of stable biexcitons.

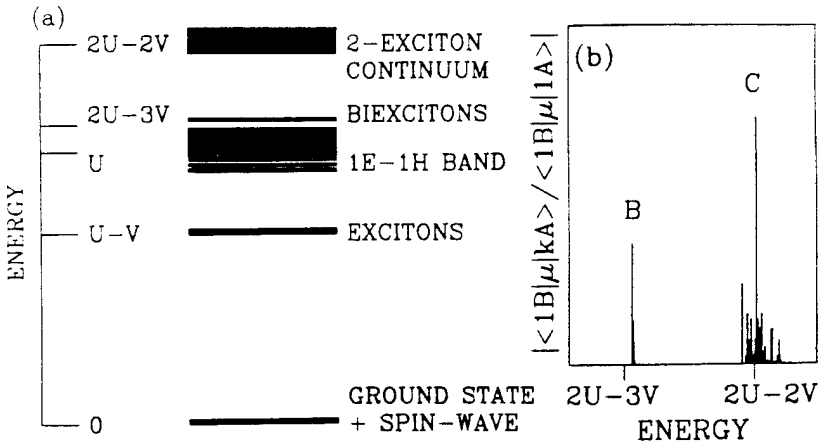

Figure 13. (a) Total energies of the N = 10 periodic ring, for U/t = 50, V/t = 15, and δ = 0.1. (b) Normalized dipole couplings between the optical exciton and the two-exciton states of (a).

Having established the validity of our physical criterion for the strong-coupling case, we now proceed to the case of more realistic parameters, U/t = 3 and V/t = 1. Calculations are now for the open chain of 10 atoms, within the quadruple CI (QCI) approximation. We start with the limit of very large and unrealistic δ, where all solutions are bandlike. In Fig. 14(a) we have plotted the normalized dipole couplings between the $1B_u$ and all excited even-parity A_g states against their normalized energies, for the parameters above. The level labeled 2 is the $2A_g$ state, level m is the mA_g state discussed previously in the context of

nonresonant nonlinear optics,[24-26] and level B is the lowest 2e-2h excitation, as evidenced by its energy of nearly 2 x E ($1B_u$), and by its normalized dipole coupling of nearly 1. Having identified the lowest 2e-2h state for the weakly correlated case, we now increase the correlation contribution to the optical gap by gradually reducing δ. For each δ we again plot the normalized dipole couplings of all excited A_g states with the $1B_u$ against their normalized energies. These results are shown in Figs. 14(b)-(d). The gradual reduction in δ along with the result of Fig. 11(a) allows us to continue to demarcate between 1e-1h and 2e-2h excitations. It is clear from Fig. 11 that the major effect of reducing δ (increasing correlations) is a redistribution of dipole moments of A_g states with the $1B_u$: the relative shifts of energy are small within this range of parameters. There should be no doubt whatsoever that in all cases the level labeled B is the lowest two-exciton state. Our interest lies in the realistic δ region (δ < 0.3) applicable to π-conjugated polymers. Note the clear emergence here of a level C above level B that is more strongly dipole coupled to the $1B_u$ than B is. As discussed above, this is a distinct signature of stable biexcitons in the long chain limit.

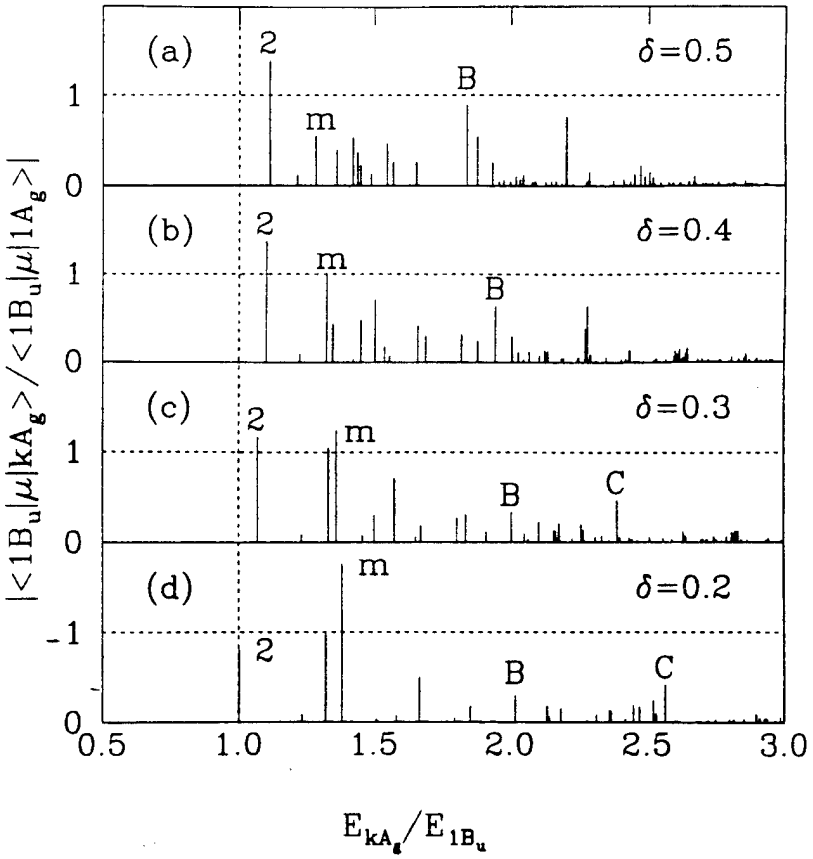

Figure 14. Dipole couplings between the $1B_u$ and all excited A_g states, normalized by the dipole coupling between the ground state and the $1B_u$, plotted against the normalized energies of the A_g states for different δ, and U/t = 3 and V/t = 1. The emergence of a level C above B for δ < 0.3 that is more strongly dipole coupled to the $1B_u$ than B indicates that B is a biexciton (see text).

The occurrence of stable biexcitons below the two-exciton continuum can explain a longstanding mystery in photophysics of conjugated polymers. In many conjugated polymers a high energy (1.4 - 1.8 eV) ps PA that is distinct from the PA due to bipolarons or triplet excitons has been observed.[31-34] No such PA is expected within single-particle electron-phonon coupled models. Our results show that within the Coulomb correlated model, a natural explanation of the PA emerges as the optical transition from the exciton to the biexciton. The occurrence of stable biexcitons also implies a novel nonlinear optical channel that would contribute to the overall third-order optical nonlinearity of these systems. The effect of this channel on the magnitude of optical nonlinearity is currently being investigated.

F. Electroabsorption in DCH-Polydiacetylene, Experiment and Theory[35]

We conducted a combined experimental and theoretical investigation to characterize the optoelectronic properties of a DCH-PDA thin film and to understand the nature of band and excitonic states. Our measured differential absorption spectra showed a Stark shift of the lowest energy exciton, accompanied by a large high-energy oscillatory signal [see Fig. 15(a) and (b)], whose origin has been a subject of controversy. Comparisons of our experimental results and exact numerical calculations [see Fig. 15(c) and (d)] indicate that the high-energy signal is due to transitions to the conduction band. This work led to our determination of the precise mechanism of third-order optical nonlinearity. It was shown that the high-energy band states play a strong role not only in electroabsorption, but in other nonlinear optical measurements as well.

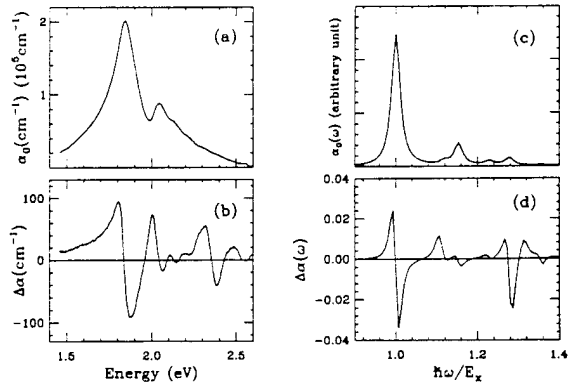

Figure 15. (a) The measured linear absorption coefficient, $\alpha_0(\omega)$, of our DCH-PDA sample. The large excitonic peak is shown with higher-energy vibronic sidebands; (b) absorption changes, $\Delta\alpha = \alpha - \alpha_0$, for a 120-kV/cm field applied to the sample with coplanar electrodes separated by 50 μm. A Stark shift of the exciton and its vibronics is clearly seen with an additional higher-energy feature beginning at 2.35 eV. (c) Calculated linear absorption in arbitrary units for the extended Hubbard Hamiltonian. (d) Calculated field-induced $\Delta\alpha$. The new feature at high energy is due to the conduction band.

G. String-Excitons in a Charge-Transfer Solid[36]

We proposed that metal-halide (M-X) chains are potentially good candidates for third-order nonlinear optical materials. There are two reasons for this. First, these materials are charge-density wave systems, as opposed to the π-conjugated polymers which are spin density wave. This implies that two-photon excitations are relatively high in energy. Secondly, both the metal and the halogen atoms are heavier than carbon, and as such, i.r. vibrations should occur at much lower energies than in carbon-based systems, thereby providing a wider frequency window for device applications.

Samples of M-X chains were synthesized. We also investigated the optical nonlinearity mechanism of a different charge density wave system which can be considered a strongly correlated model for the M-X chains. We have made the first observation and provided a theoretical description of multiexciton states in an organic CT solid. Binding of more than two excitons is not possible with conventional semiconductors. This is not true in one-dimensional strongly correlated materials, where the CT excitons are bound due to the combined effects of strong Coulomb interaction and one-dimensional confinement.

In order to verify the occurrence of the multiexciton states, we carried out differential transmission measurements on Anthracene-PMDA. At low pump photon intensities, photo-induced absorption to only the 2-exciton (biexciton) is observed. At higher intensities a new photo-induced absorption develops at even lower energy. This has been explained as absorption from the 2-exciton to a stable 3-exciton within our theoretical calculation. The experimental and theoretical results are compared in Fig. 16.

Similar multiexcitons may also be stable in the M-X chains, in which case they will strongly influence the nonlinear optical behavior of these materials.

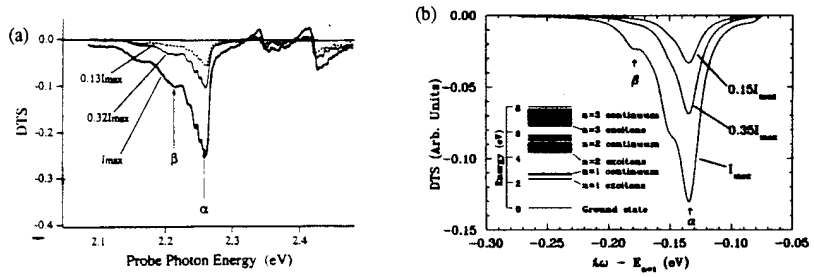

Figure 16. (a) The differential transmission spectrum (DTS) at three different pump intensities; I_{max} corresponds to the maximum pump fluence of 1 mJ cm^{-2}. Note that the induced absorption " appears at all pump intensities, while a second induced absorption β appears only at strong intensities. (b) Calculated DTS in a strongly neutral CT solid for different pump intensities I. The inset shows the energy spectrum. The calculations were done for a periodic ring of 14 sites, with t = -0.1 eV, V_1 = 0.5 eV, $V_{|m|} = V_1/m$, and ε = 1.38 eV. The above magnitudes of t and V_1 are typical for CT solids, whereas , was chosen to fit the experimental energy of the 1-exciton. Note that the calculation reproduces the induced absorptions α and β seen in the experiment. The larger energy shifts in the calculated DTS compared to the experiment are finite-size effects.

H. Organic Superlattices of PTCDA and InPc-Cl - 'Exciton Confinement'? and Charge/Energy Transfer

In order to elucidate the excitonic dynamics in organic superlattices of PTCDA and InPc-Cl, we prepared periodic multilayers of these materials on epitaxial sapphire substrates. Figure 17 shows the result of the linear absorbance measurements for four samples where the monolayers (MLs) were changed from one to four.

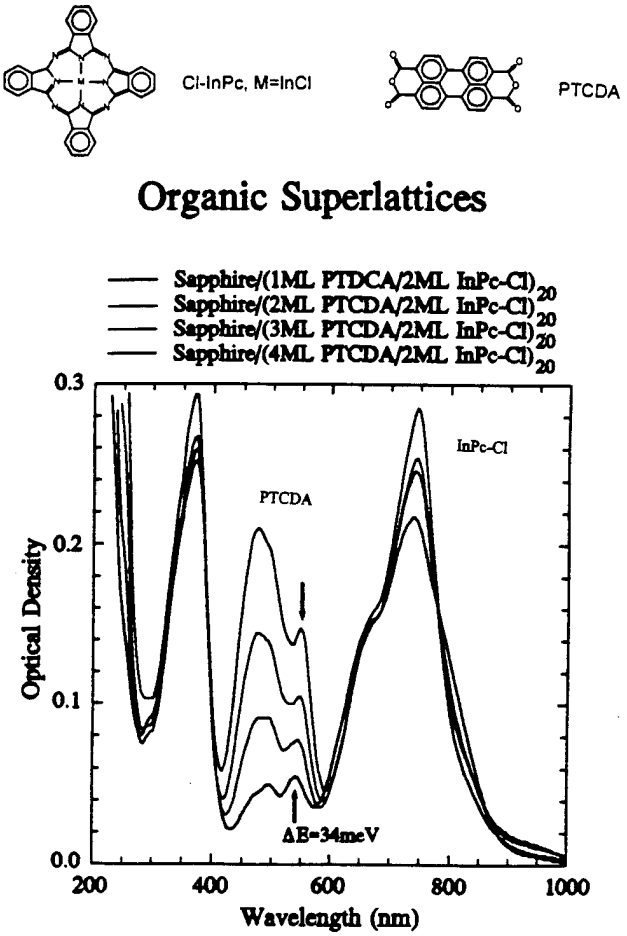

Figure 17. Chemical structure of InPc-Cl and PTCDA and linear absorbance of different periodic multilayers of the type sapphire/ (x ML PTCDA / y ML InPc-Cl)$_{20}$. Note the blue shift in the exciton position (arrows) for decreasing PTCDA thickness.

The molecular excitonic feature of the PTCDA spectra (marked by arrows in Fig. 16) is shifted to higher energies with decreasing PTCDA thickness (blue-shift). This result is important because similar findings of an increase in energy with decreasing width in a quantum well are discussed as "exciton confinement."[37] Whether our multilayer thin films show the same ordering as previous PTCDA/NTCDA[37]

is not clear. However, the fact that we see a blue-shift in the PTCDA spectrum comparable to these earlier results is a strong hint that the explanation of this result by quantum confinement of the PTCDA excitons is not necessary. We believe that the blue-shift is caused by the changing polarization environment that the PTCDA molecules experience with decreasing layer thickness (Frenkel exciton model). We have been able to calculate such peak shifts in films of phthalocyanines from the measured architecture of the film and expect a similar relationship in perylene dye films.

The dynamics of the exciton in the periodic multilayers was investigated with the help of femtosecond pump probe spectroscopy. It was shown that when pumped at the wavelength of the PTCDA exciton, energy or charge is transferred to the phthalocyanine layers. This is visible in the experiments as a delayed bleaching at the InPc-Cl absorbance maximum.

References

1. K. Meerholz, B. L. Volodin, Sandalphon, B. Kippelen, and N. Peyghambarian, Nature **371**, 497 (1994).
2. N. Peyghambarian, K. Meerholz, B. Volodin, Sandalphon, and B. Kippelen, Optics & Photonics News **15**, 13 (1994); W. E. Moerner and N. Peyghambarian in Optics and Photonics News **6**, 24 (1995).
3. R. Dagani, C&EN , pg. 28, Feb. 20, 1995
4. B. G. Levi, Physics Today **48**, 17 (1995).
5. B. Kippelen, B. L. Volodin, Sandalphon, K. Meerholz, and N. Peyghambarian, CLEO '95, 1995 Technical Digest Series **15**, 164 (1995).
6. K. Meerholz, B. Kippelen, and N. Peyghambarian, The Spectrum **8**, 1 (1995).
7. C. C. Teng and H. T. Man, Appl. Phys. Lett. **56**, 1734 (1990).
8. C. Halvorson, B. Kraabel, A. J. Heeger, B. L. Volodin, K. Meerholz, Sandalphon, and N. Peyghambarian, Opt. Lett. **20**, 76 (1995).
9. B. L. Volodin, K. Meerholz, Sandalphon, B. Kippelen, N. V. Kukhtarev, and N. Peyghambarian, Opt. Eng. **34**, 2213 (1995).
10. A. Schmidt, R. Schlaf, D. Louder, L.-K. Chau, S.-Y. Chen, T. Fritz, M. F. Lawrence, B. A. Parkinson, and N. Armstrong, submitted to Chemistry of Materials.
11. T. Schuerlein, A. Schmidt, P. A. Lee, K. W. Nebesny, and N. Armstrong, invited paper for Jap. J. Appl. Phys. (in press).

12. Schmidt, T. J. Schuerlein, G. E. Collins, and N. Armstrong, J. Phys. Chem. (in press).
13. A. Schmidt, A. Back, L.-K. Chau, and N. Armstrong, "Organic Molecular Beam Epitaxy of Phthalocyanine and Naphthalocyanine Ultrathin Films," invited chapter in *Phthalocyanines*, edited by C. A. Leznoff, and A. P. B. Lever (VCH Publications, 1995).
14. H. Tajalli, J. P. Jiang, A. Schmidt, J. T. Murray, M. Chandross, S. Mazumdar, N. Peyghambarian, and N. Armstrong, Appl. Phys. Lett. **67**, 1639 (1995).
15. Z. Z. Ho and N. Peyghambarian, Chem. Phys. Lett. **148**, 107 (1988).
16. J. S. Shirk, J. R. Lindle, F. J. Bartoli, C. A. Hoffman, Z. H. Kafafi, and A. W. Snow, Appl. Phys. Lett. **55**, 1287 (1989).
17. L. K. Chau, C. D. England, S. Chen, and N. R. Armstrong, J. Phys. Chem. **97**, 2699 (1993).
18. J. P. Jiang, H. Tajalli, J. T. Murray, S. Mazumdar, A. Schmidt, N. R. Armstrong, and N. Peyghambarian, QMA7, CLEO, 1995.
19. A. M. Schaffer and M. Gouterman, Theoret. Chim. Acta **25**, 62 (1972).
20. E. Orti, J. L. Bredas, and C. Clarisse, J. Chem. Phys. **92**, 1228 (1990).
21. Y. Iwasa, E. Funatsu, T. Hasegawa, T. Koda, and M. Yamashita, Appl. Phys. Lett. **59**, 2218 (1991).
22. M. Chandross, S. Mazumdar, S. Jeglinski, X. Wei, and Z.V. Vardeny, Phys. Rev. B **50**, 14702 (1994).
23. M. Chandross, F. Guo, and S. Mazumdar, Synth. Metals **69**, 625 (1995).
24. D. Guo, S. Mazumdar, and S. N. Dixit, Nonlin. Opt. **6**, 337 (1994).
25. D. Guo, S. Mazumdar, S. N. Dixit, F. Kajzar, F. Jarka, Y. Kawabe, and N. Peyghambarian, Phys. Rev. B **48**, 1433 (1993).
26. S. Mazumdar and F. Guo, J. Chem. Phys. **100**, 1665 (1994).
27. S. Mazumdar, D. Guo, and S. N. Dixit, Synth. Metals **55-57**, 3881 (1993).
28. J. M. Leng, S. Jeglinski, X. Wei, Z. V. Vardeny, R. E. Benner, F. Y. Guo, and S. Mazumdar, Phys. Rev. Lett. **72**, 156 (1994).
29. F. Guo, M. Chandross, and S. Mazumdar, Phys. Rev. Lett. **74**, 2086 (1995).
30. F. Guo, M. Chandross, and S. Mazumdar, Mol. Cryst. Liq. Cryst. **256**, 53 (1994).
31. M. B. Sinclair et al., Synth. Metals **50**, 593 (1992).
32. T. Kobayashi et al., J. Opt. Soc. Am B **7**, 1558 (1990).

33. J. W. P. Hsu et al., Phys. Rev. B **49**, 712 (1994).

34. J. M. Leng et al., Mol. Cryst. Liq. Cryst. **256**, 697 (1994).

35. D. Guo, S. Mazumdar, S. N. Dixit, F. Kajzar, F. Jarka, Y. Kawabe, and N. Peyghambarian, Phys. Rev. B **48**, 1433 (1993).

36. M. Kuwata-Gonokami, N. Peyghambarian, K. Meissner, B. Fluegel, Y. Sato, K. Ema, R. Shimano, S. Mazumdar, F. Guo, T. Tokihiro, H. Ezaki, and E. Hanamura, Nature **367**, 47 (1994); H. Ezaki, T. Tokihiro, M. Kuwata-Gonokami, R. Shimano, K. Ema, E. Hanamura, B. Fluegel, K. Meissner, S. Mazumdar, and N. Peyghambarian, Solid State Commun. **88**, 211 (1993).

37. F. F. So and S. R. Forrest, Phys. Rev. Lett. **66**, 2649 (1991); F. F. So and S. R. Forrest, Mo.. Cryst. Liq. Cryst. Sci. Technol. B **2**, 205 (1992).

List of Publications During this Reporting Period

1. R. Dagani, C&EN, pg.28, Feb. 20, 1995.
2. B. Kippelen, B. L. Volodin, Sandalphon, K. Meerholz, and N. Peyghambarian, CLEO '95, 1995 Technical Digest Series **15**, 164 (1995).
3. K. Meerholz, B. Kippelen, and N. Peyghambarian, The Spectrum **8**, 1 (1995).
4. C. Halvorson, B. Kraabel, A.J. Heeger, B. L. Volodin, K. Meerholz, Sandalphon, and N. Peyghambarian, Opt. Lett. **20**, 76 (1995).
5. B. L. Volodin, K. Meerholz, Sandalphon, B. Kippelen, N. V. Kukhtarev, and N. Peyghambarian, to appear in Opt. Eng. **34**, 2213 (1995).
6. A. Schmidt, R. Schlaf, D. Louder, L.-K. Chau, S.-Y. Chen, T. Fritz, M. F. Lawrence, B. A. Parkinson, and N. Armstrong, submitted to Chemistry of Materials.
7. T. Schuerlein, A. Sehmidt, P. A. Lee, K. W. Nebesny, and N. Armstrong, invited paper for Jap. J. Appl. Phys. (in press).
8. A. Schmidt, T. J. Schuerlein, G. E. Collins, and N. Armstrong, J. Phys. Chem. (in press).
9. A. Schmidt, A. Back, L.-K. Chau, and N. Armstrong, "Organic molecular beam epitaxy of phthalocyanine and naphthalocyanine ultrathin films," invited chapter in *Phthalocyanines,* edited by C. A. Leznoff and A. P. B. Lever (VCH Publications, 1995).

10. J. P. Jiang, H. Tajalli, J. T. Murray, S. Mazumdar, A. Schmidt, N. R. Armstrong, and N. Peyghambarian, QMA7, CLEO, 1995.
11. H. Tajalli, J. P. Jiang, A. Schmidt, J. T. Murray, M. Chandross, S. Mazumdar, N. Peyghambarian, and N. Armstrong, Appl. Phy. Lett. **67**, 1639 (1995).
12. N. Peyghambarian, K. Meerholz, B. Volodin, Sandalphon, and B. Kippelen, Optics & Photonics News **15**, 13 (1994); W.E. Moerner and N. Peyghambarian in Optics and Photonics News **6**, 24 (1995).
13. M. Chandross, F. Guo, and S. Mazumdar, Synth. Metals **69**, 625 (1995).
14. F. Guo, M. Chandross, and S. Mazumdar, Phys. Rev. Lett. **74**, 2086 (1995).
15. S. Mazumdar and M. Chandross, "Theory of photoexcitations in the polyphenylenes," Proceeding of SPIE Conference 2528.
16. S. Mazumdar and F. Guo, "Theory of biexcitons in mixed and segregated stack charge-transfer solids, molecular crystals, and π-conjugated polymers," Proceedings of *Charge Transport in Electric Polymers,* May 1995, to be published in Synth. Metals.
17. B. Kippelen, K. Meerholz, and N. Peyghambarian, "An introduction to photorefractive polymers," edited by H. S. Nalwa (CRC Press).
18. N. Peyghambarian, B. Kippelen, and K. Meerholz, Chemistry and Industry (in press).
19. K. Meerholz, B. L. Volodin, Sandalphon, B. Kippelen, and N. Peyghambarian, Nature **371**, 497 (1994).
20. M. Chandross, S. Mazumdar, S. Jeglinski, X. Wei, and Z. V. Vardeny, Phys. Rev. B **50**, 14702 (1994).
21. D. Guo, S. Mazumdar, and S. N. Dixit, Nonlin. Opt. **6**, 337 (1994).
22. J. M. Leng, S. Jeglinski, X. Wei, Z. V. Vardeny, R. E. Benner, F. Y. Guo, and S. Mazumdar, Phys. Rev. Lett. **72**, 156 (1994).
23. S. Mazumdar, and F. Guo, J. Chem. Phys. **100**, 1665 (1994).
24. F. Guo, M. Chandross, and S. Mazumdar, Mol. Cryst. Liq. Cryst. **256**, 53 (1994).
25. M. Kuwata Gonokami, N. Peyghambarian, K. Meissner, B. Fluegel, Y. Sato, K. Ema, R. Shimono, S. Mazumdar, F. Guo, T. Tokihiro, H. Ezaki, and E. Hanamura, Nature (London) **367**, 47 (1994).
26. F. Y. Guo, D. Guo, and S. Mazumdar, Phys. Rev. B **49**, 10102 (1994).

27. J. M. Leng, D. Dick, X. Wei, Z. V. Vardeny, F. Guo, and S. Mazumdar, "Excited energy states in poly(p-phenylenevinylene)," in Proceedings of *Optical Probes of Conjugated Polymers and Fullerenes,* Salt Lake City, Utah, Febuary 1994; Molecular Crystals and Liquid Crystals **256**, 1 (1994).

28. D. Guo, S. Mazumdar, S. N. Dixit, F. Kajzar, F. Jarka, Y. Kawabe, and N. Peyghambarian, Phys. Rev. B **48**, 1433 (1993).

29. S. Mazumdar, D. Guo, and S. N. Dixit, Synth. Metals **55**, 3881 (1993).

30. Sandalphon, B. Kippelen, N. Peyghambarian, S. R. Lyon, A. B. Padias, and H. K. Hall, Jr., Opt. Lett. **19**, 68 (1994).

31. N. Peyghambarian, "Exiton strings in an organic charge transfer crystal," *Workshop on Microprocessing and Microsystems,* Schloss Ringberg, Tegernsee, Germany, June 19-23, 1994.

32. N. Peyghambarian, B. Fluegel, K. Meissner, F. Guo, S. Mazumdar, M. Kuwata-Gonokami, Y. Sato, K. Ema. R. Shimano, T. Tokihiro, H. Ezaki, and E. Hanamura, "Observation of excitonic strings in a quasi-one-dimensional charge transfer crystal," IQEC '94, Anaheim, California, May 8-13, 1994.

33. N. Peyghambarian, "Highly efficient photorefractive polymer composites," American Chemical Society/Optical Society of America, Conference on *Polymeric Thin Films for Photonics Applications*, Washington, DC, Aug. 21-24, 1994.

34. N. Peyghambarian, "Photorefractive polymers and multiexcitonic states in organics," Second International Topical Conference on *Optical Probes of Conjugated Polymers and Fellerenes,* Salt Lake City, Utah, Feb. 15-19, 1994.

35. K. Meerholz, B. Volodin, Sandalphon, B. Kippelen, and N. Peyghambarian, " A new highly efficient PVK-based photorefractive polymer," OSA Annual Meeting, Dallas, Texas, Oct. 1994.

36. A. Schmidt, V. S. Williams, L. Chau, N. R. Armstrong, J. P. Jiang, N. Peyghambarian, and S. Mazumdar, "Epitaxial Growthof InPc-Cl and AIPc-F on SnS_2 and KBR-influence of crystalline morphology and structurre on linear and nonlinear optical properties," proceedings of 1994 MRS Fall Meeting, Boston, Massachusetts.

37. B. Kippelen, Sandalphon, K. meerholz, B. Volodin, and N. Peyghambarian, "New highly efficient photorefractive polymer composites," ICON'1, Val-Thorens, France, Jan. 9-13, 1994.

38. H. Ezaki, T. Tokihiro, M. Kuwata Gonokami, R. Shimano, K. Ema, E. Hanamura, B. Fluegel, K. Meissner, S. Mazumdar, and N. Peyghambarian, Solid State Commun. **88**, 211 (1993).

39. L. K. Chau, C.D. England, S. Chen, and N. R. Armstrong, J. Phys. Chem. **97**, 2699 (1993).

40. B. Kippelen, K. Tamura, n. Peyghambarian, A. B. Padias, and H. K. Hall, Jr., J.Appl. Phys. **74**, 1, (1993).

41. B. Kippelen, K. Tamura, N. Peyghambarian, A. B. Padias, and H. K. Hall, Jr., Phys. Rev. B **48**, 10710 (1993).

42. N. Peyghambarian, S. W. Koch, and A. Mysyrowicz, *Introduction to Semiconductor Optics* (Prentice Hall, Englewood Cliffs, 1993).

43. G. E. Collins, V. S. Williams, L.-K. Chau, K. W. Nebesny, C. England, P.A. Lee, T. Lowe, and Q. Fernando, Synthetic Metals **54**, 351 (1993).

44. B. Kippelen, Sandalphon, N. Peyghambarian, S. R. Lyon, A. B. Padias, and H. K. Hall, Electron. Lett. **29**, 1873 (1993).

45. V. Williams, Sandalphon, S. MAzumdar, C. D. England, M. L. Anderson, N. Armstrong, and N. Peyghambarian, "Biexcitonic absorption in an epitaxial chloro-indium phthalocyanine thin film," QELS '93, Baltimore, Maryland, May 2-7, 1993, paper QTuE6.

46. B. Kippelen, Sandalphon, N. Peyghambarian, S. R. Lyon, A. B. Padias, and Hank Hall, Jr.,"AZO-dyed-doped photoreefractive polymers," proceedings of ACS/OSA Topical Meeting on *Organic Thin Films for Photonic Applications,* Toronto, Canada, Oct. 6-8, 1993.

47. Sandalphon, B. Kippelen, K. Meerholz, B. Volodin, and N. Peyghambarian, "High diffractrion efficiency and net gain in a new PVK-based photorefractive polymer composite," postdeadline paper for ILS-IX Conference, Toronto, Canada, Oct. 3-8, 1993, PDP2-1.

48. V. S. Willaims, N. R. Armstrong, A. Schmidt, M. L. anderson., L.-K. Chau, Sandalphon, and N. Peyghambarian, and S. Mazumdar, "Organic molecular beam epitaxy: formation and characterization of ordered organic/semiconductor heterojunctions and organic/organic superlattices," proceedings of 1993 MRS Fall Meeting, Boston, Massachusetts.

49. B. Kippelen, Sandalphon, N. Peyghambarian, S. R. Lyon, A. B. Padias, and H. K. Hall, Jr.,"Photorefractivity and photo-isomerization in azo-dye-doped polymers," proceedings of 1993 MRS Fall Meeting, Boston, Massachusetts.

50. S. Mazumdar and N. Peyghambarian, "Covalent states, excitons, bands, and biexcitons in π-and σ-conjugated materials," proceedings of 1993 MRS Fall Meeting, Boston, Massachusetts.

51. N. Peyghambarian, K. Meissner, B. Fluegel, S. Mazumdar, F. Guo, M. Kuwata-Gonokami, Y. Sato, K. Ema, R. Shimano, T. Tokihiro, H. Ezaki, and E. Hanamura, "Observation of excitonic n-strings in a quasi-one-dimensional charge-transfer crystal," proceedings of 1993 MRS Fall Meeting, Boston, Massachusetts, paper Q13.10.